

COMPARISON OF SOLVERS FOR 2D SCHRÖDINGER PROBLEMS

F.J. GASPAR, C. RODRIGO, R. ČIEGIS, AND A. MIRINAVIČIUS

Abstract. This paper deals with the numerical solution of both linear and non-linear Schrödinger problems, which mathematically model many physical processes in a wide range of applications of interest. In particular, a comparison of different solvers and different approaches for these problems is developed throughout this work. Two finite difference schemes are analyzed: the classical Crank-Nicolson approach, and a high-order compact scheme. Solvers based on geometric multigrid, Fast Fourier Transform and Alternating Direction Implicit methods are compared. Finally, the efficiency of the considered solvers is tested for a linear Schrödinger problem, proving that the computational experiments are in good agreement with the theoretical predictions. In order to test the robustness of the MG solver two additional Schrödinger problems with a non-constant potential and nonlinear right-hand side are solved by the MG solver, since the efficiency of this solver depends on such data.

Key words. finite difference method, Schrödinger problem, multigrid method, Alternating Direction Implicit method, Fast Fourier Transform method.

1. Introduction

It is well-known that many mathematical problems of nonlinear optics, laser physics and quantum mechanics, for example, are described by Schrödinger problems. Therefore, the development of robust and efficient numerical algorithms for the solution of such problems still remains a very important challenge of computational mathematics. In particular, one of the most important aspects in the numerical solution of partial differential equations is the efficient solution of the corresponding large system of equations arising from their discretization.

Three different strategies are very popular for this purpose. The first strategy is based on operator splitting techniques. The main idea is to decompose the large system of linear equations arising after the discretization of a multidimensional problem to a sequence of simpler subproblems. Within this framework, here we only mention Alternating Direction Implicit (ADI), Locally One-Dimensional (LOD) and Implicit-Explicit (IMEX) methods (see [16, 20] for a good review on these methods). Secondly, we mention Fast Fourier Transform (FFT) techniques. The FFT algorithm was introduced in 1965 by Cooley and Tukey [12], for an overview of Fourier Transform methods we refer e.g. to [13]. In the case of PDEs with constant coefficients and uniform grids, these algorithms solve systems of linear equations with complexity close to optimal. Thus, we include solvers based on the FFT algorithm into the comparison of different solvers for 2D Schrödinger problems. The third class of solvers corresponds to multigrid (MG) methods. Since their development in the 70's, MG methods [5, 25] have been proved to be among the most efficient numerical algorithms for solving the large sparse systems of algebraic equations arising from the discretization of elliptic PDEs, achieving asymptotically

Received by the editors September 17, 2012 and, in revised form, May 5, 2013.

2000 *Mathematics Subject Classification.* 35R35, 49J40, 60G40.

This research was partially supported by FEDER/MCYT Projects MTM 2010-16917 and the DGA (Grupo consolidado PDIE).

optimal complexity. They are mainly based on the acceleration of the convergence of common iterative methods by using solutions obtained on coarser meshes as corrections. We note that MG solvers are not frequently used to solve Schrödinger type problems in industrial and academic applications.

Our aim in this paper is to investigate in detail the possibility of constructing robust and efficient MG solvers and compare these solvers with those based on ADI and FFT techniques. The biggest challenge is the development of robust MG solvers for multidimensional Schrödinger problems. There are not many papers devoted to this topic. We note, that similar challenges arise in application of MG solvers for the Helmholtz equation [14, 18].

The rest of the paper is organized as follows. In Section 2 the mathematical model is formulated and the main properties of the solution are given. The two-dimensional Schrödinger equation is approximated by the classical Crank-Nicolson method and by a high-order compact finite difference scheme in space. For the solution of the high-order scheme, an ADI type decomposition algorithm, from [15], is used. The stability and convergence analysis in the discrete L_2 norm of the high-order ADI scheme is done in Section 3, whereas the MG solver for Schrödinger problem is described and investigated in Section 4. Results of numerical experiments are presented in Section 5. Finally, in Section 6 some conclusions are formulated.

2. Problem Formulation

2.1. Mathematical model. For many applications in nonlinear optics, laser physics, quantum mechanics and plasma physics, for instance, the mathematical models of physical processes are described by nonlinear Schrödinger equations, see, e.g., [11, 16] and references therein. We consider the two-dimensional nonlinear Schrödinger equation in the domain $\Omega = (a_x, b_x) \times (a_y, b_y)$:

$$(1) \quad -i \frac{\partial u}{\partial t} = \frac{\partial^2 u}{\partial x^2} + \frac{\partial^2 u}{\partial y^2} - q(x, y)u + f(u), \quad (x, y) \in \Omega, \quad t \in (0, T],$$

with the following initial and boundary conditions

$$(2) \quad u(x, y, 0) = u_0(x, y), \quad (x, y) \in \Omega \cup \partial\Omega,$$

$$(3) \quad u(x, y, t) = \mu(x, y, t), \quad (x, y) \in \partial\Omega, \quad t \in (0, T].$$

Here $u = u(x, y, t)$ is a complex-valued function, q is a given real-valued function, f , u_0 and μ are given complex-valued functions, and $\partial\Omega$ is the boundary of Ω .

It is well-known that the nonlinear Schrödinger equation (1) can have important conservation laws. Let us assume that $f(u) \equiv 0$. The following invariants of the solution of (1)–(3) are valid under the assumption of homogeneous boundary conditions $\mu \equiv 0$ [9, 27]:

$$(4) \quad Q = \int_{\Omega} |u(x, y, t)|^2 dx dy = \int_{\Omega} |u_0(x, y)|^2 dx dy,$$

$$(5) \quad E = \int_{\Omega} \left(\left| \frac{\partial u(t)}{\partial x} \right|^2 + \left| \frac{\partial u(t)}{\partial y} \right|^2 + q(x, y)|u(t)|^2 \right) dx dy$$

$$= \int_{\Omega} \left(\left| \frac{\partial u_0}{\partial x} \right|^2 + \left| \frac{\partial u_0}{\partial y} \right|^2 + q(x, y)|u_0|^2 \right) dx dy.$$

2.2. Finite difference schemes. There are many numerical algorithms for the solution of the nonlinear Schrödinger problem. They are based on finite-difference schemes (see, e.g., [2, 9, 11, 21, 23]), finite-element and Galerkin approaches (see, [1, 2]), or spectral and pseudo-spectral methods. In this section we restrict ourselves to finite difference schemes, and our main goal is to compare solvers for the large systems of linear equations obtained after the discretization step. Note that the main properties of such systems are very similar for all mentioned methods.

The considered domain $\bar{\Omega} := \Omega \cup \partial\Omega$ is covered by the following discrete uniform grid

$$\bar{\Omega}_h = \{(x_j, y_k) : x_j = a_x + jh, \quad y_k = a_y + kh, \quad j = 0, \dots, J, \quad k = 0, \dots, K\},$$

$x_J = b_x$, $y_K = b_y$, $\bar{\Omega}_h = \Omega_h \cup \partial\Omega_h$, with the grid points denoted by (x_j, y_k) . Let ω_τ be a uniform time grid $\omega_\tau = \{t^n : t^n = n\tau, n = 0, \dots, N, N\tau = T\}$, where τ is the time step. Although the constant time step is considered here, the following studies can be easily extended to the case when τ varies. Adaptive time-stepping strategies can be used. But the main aim of this paper is to compare efficiency and robustness of the MG solver for multidimensional Schrödinger problems, when the full approximation algorithms are used. The robustness of the solver with respect to time-stepping parameter is one of the important features of general solvers.

We consider numerical approximations U_{jk}^n to the exact solution values $u_{jk}^n = u(x_j, y_k, t^n)$ at the grid points $(x_j, y_k, t^n) \in \bar{\Omega}_h \times \omega_\tau$. The following notations for difference and averaging in time operators are used [15]:

$$\begin{aligned} \partial_x U_{jk}^n &= (U_{j+1,k}^n - U_{jk}^n)/h, & \partial_y U_{jk}^n &= (U_{j,k+1}^n - U_{jk}^n)/h, \\ \partial_t U_{jk}^n &= (U_{jk}^{n+1} - U_{jk}^n)/\tau, & U_{jk}^{n+1/2} &= (U_{jk}^{n+1} + U_{jk}^n)/2, \\ \partial_x^2 U_{jk}^n &= \frac{U_{j+1,k}^n - 2U_{jk}^n + U_{j-1,k}^n}{h^2}, & \partial_y^2 U_{jk}^n &= \frac{U_{j,k+1}^n - 2U_{jk}^n + U_{j,k-1}^n}{h^2}, \end{aligned}$$

and therefore, the standard Crank-Nicolson scheme is given as follows:

$$\begin{aligned} (6) \quad & -i\partial_t U_{jk}^n = \partial_x^2 U_{jk}^{n+1/2} + \partial_y^2 U_{jk}^{n+1/2} - q_{jk} U_{jk}^{n+1/2} + f(U_{jk}^{n+1/2}), \\ & (x_j, y_k) \in \bar{\Omega}_h, \quad t^n \in \omega_\tau, \\ & U_{jk}^0 = u_0(x_j, y_k), \quad (x_j, y_k) \in \bar{\Omega}_h, \\ & U_{jk}^n = \mu(x_j, y_k, t^n), \quad (x_j, y_k) \in \partial\Omega_h, \quad t^n \in \omega_\tau. \end{aligned}$$

The convergence of a discrete solution of the Crank-Nicolson scheme (6) has been well-investigated and the second-order accuracy of this approach has been proved in various norms, see, e.g., [1, 21] and references therein.

Instead of the finite difference method, the diffraction operator can be approximated by the finite-element Galerkin type methods (see [1, 2]). But for the application of MG and FFT solvers the obtained systems of discrete equations have very similar properties to those systems generated by the finite difference method.

Let $H_0(\Omega_h)$ denote the set of grid functions V defined on $\bar{\Omega}_h$ with $V = 0$ on $\partial\Omega_h$. Now, we define some discrete inner products and norms on $H_0(\Omega_h)$ as follows:

$$\begin{aligned} (V, W)_h &= \sum_{j=1}^{J-1} \sum_{k=1}^{K-1} V_{jk} \bar{W}_{jk} h^2, & \|V\| &= \sqrt{(V, V)_h}, \\ (V, W)_x &= \sum_{j=0}^{J-1} \sum_{k=1}^{K-1} V_{jk} \bar{W}_{jk} h^2, & (V, W)_y &= \sum_{j=1}^{J-1} \sum_{k=0}^{K-1} V_{jk} \bar{W}_{jk} h^2, \\ \|V\|_x &= \sqrt{(V, V)_x}, & \|V\|_y &= \sqrt{(V, V)_y}, & \|V\|_E^2 &= \|\partial_x V\|_x^2 + \|\partial_y V\|_y^2, \end{aligned}$$

where \bar{W}_{jk} denotes the complex-conjugate of W_{jk} .

We consider the high-order compact finite difference scheme investigated in [15]. Let us introduce the operators

$$\mathcal{L}_x U_{jk}^n = \left(1 + \frac{h^2}{12} \partial_x^2\right) U_{jk}^n, \quad \mathcal{L}_y U_{jk}^n = \left(1 + \frac{h^2}{12} \partial_y^2\right) U_{jk}^n.$$

By using a Taylor expansion, it is easy to get that

$$\mathcal{L}_x \left(\frac{\partial^2 u}{\partial x^2}\right)_{jk}^n = \partial_x^2 u_{jk}^n + \mathcal{O}(h^4), \quad \mathcal{L}_y \left(\frac{\partial^2 u}{\partial y^2}\right)_{jk}^n = \partial_y^2 u_{jk}^n + \mathcal{O}(h^4).$$

The Crank-Nicolson implicit high-order compact scheme is given by the following discrete equation, which is also called Numerov's scheme, see [15, 17]:

$$\begin{aligned} (7) \quad & -i\mathcal{L}_x \mathcal{L}_y \partial_t U_{jk}^n = \mathcal{L}_y \partial_x^2 U_{jk}^{n+1/2} + \mathcal{L}_x \partial_y^2 U_{jk}^{n+1/2} \\ & - \mathcal{L}_x \mathcal{L}_y \left(q_{jk} U_{jk}^{n+1/2} - f(U_{jk}^{n+1/2})\right), \quad (x_j, y_k) \in \Omega_h, \quad t^n \in \omega_\tau. \end{aligned}$$

By using a Taylor expansion one can see that scheme (7) has a truncation error of $\mathcal{O}(\tau^2 + h^4)$.

As was stated above the main goal of this paper is to study the efficiency and robustness of the MG and FFT solvers for the full approximation algorithms. But we note that there are various techniques to construct time-splitting integrators for discrete schemes used to solve multidimensional nonlinear Schrödinger problems. The main idea is to reduce an implementation of the discrete scheme to a sequence of simple systems with tridiagonal matrices. We are interested in the Strang type second-order symmetrical splitting techniques. The standard operator splitting can be used to separate the linear diffraction and reaction processes. This part of splitting approach is well investigated in many papers and books, where the first, second and high order approximations are constructed and investigated, see [4, 16, 19, 22, 24]. The overview of recent results in this field is done in [10], where also schemes for 3D problems are investigated. Another way of increasing the order of the scheme in time is to do Richardson extrapolation [16]. This method can be included directly into the framework of full approximation schemes considered in our paper. We note that the analysis and a detailed comparison of different techniques for time-stepping is out of the scope of this paper.

In order to get the benchmark for the comparison of the MG solver with the time-splitting algorithms, we consider an ADI type algorithm, since the complexity of all algorithms in this class is of the same order. In [15], the ADI method was applied to split the finite difference scheme (7). Here, we adapt this method to equations with a linear (or linearized) potential $q(x, y)u$. First, the discrete equation is written in

the canonical form of two-step schemes

$$-i \left[\mathcal{L}_x \mathcal{L}_y - i \frac{\tau}{2} \left(\mathcal{L}_y \partial_x^2 + \mathcal{L}_x \partial_y^2 - \mathcal{L}_x \mathcal{L}_y Q \right) \right] \partial_t U_{jk}^n = \mathcal{L}_y \partial_x^2 U_{jk}^n + \mathcal{L}_x \partial_y^2 U_{jk}^n - \mathcal{L}_x \mathcal{L}_y \left(q_{jk} U_{jk}^n - f(U_{jk}^{n+1/2}) \right),$$

where operator Q is defined by $QU_{jk}^n = q_{jk}U_{jk}^n$. Next, we perturb the operator at $\partial_t U_{jk}^n$ and factorize it, thus, we get the following factorized difference scheme

$$(8) \quad -i \left(\mathcal{L}_x - i \frac{\tau}{2} \partial_x^2 \right) \left(\mathcal{L}_y - i \frac{\tau}{2} \left[\partial_y^2 - \mathcal{L}_y Q \right] \right) \partial_t U_{jk}^n = \mathcal{L}_y \partial_x^2 U_{jk}^n + \mathcal{L}_x \partial_y^2 U_{jk}^n - \mathcal{L}_x \mathcal{L}_y \left(q_{jk} U_{jk}^n - f(U_{jk}^{n+1/2}) \right).$$

It can be efficiently implemented in two splitting steps:

$$(9) \quad -i \left(\mathcal{L}_x - i \frac{\tau}{2} \partial_x^2 \right) \widehat{U}_{jk}^n = \mathcal{L}_y \partial_x^2 U_{jk}^n + \mathcal{L}_x \partial_y^2 U_{jk}^n - \mathcal{L}_x \mathcal{L}_y \left(q_{jk} U_{jk}^n - f(U_{jk}^{n+1/2}) \right), \quad (x_j, y_k) \in \Omega_h,$$

$$(10) \quad \left(\mathcal{L}_y - i \frac{\tau}{2} \left[\partial_y^2 - \mathcal{L}_y Q \right] \right) \partial_t U_{jk}^n = \widehat{U}_{jk}^n, \quad (x_j, y_k) \in \Omega_h,$$

and at each step only tridiagonal systems are solved.

3. Stability and Convergence Analysis of Fourth-order ADI Scheme

In [15], the stability analysis of nonlinear ADI compact difference scheme is done by using energy estimates. For constant $q \equiv 0$, it is proved that the solution of scheme (9)–(10) is stable if $\tau < h^2/12$ and it converges to the exact solution of differential problem (1)–(3), the error in the L_2 norm can be bounded by $C(\tau^2 + h^4)$. The validity of conservation laws is investigated numerically in [15], and it is shown that the discrete versions of integrals (4) and (5) are quite well preserved for $t^n > 0$. In this section, we apply the spectral stability analysis. Let us consider the homogeneous problem, that is, $f \equiv 0$ and $\mu \equiv 0$, and let us assume that $q = q(x, t)$ is constant.

Our first goal is to investigate the stability of the ADI scheme (9)–(10) with respect to the initial condition. Let λ_j be eigenvalues of operators ∂_x^2 and ∂_y^2 , then the following estimates are valid (see [20]): $8 \leq \lambda_j \leq 4/h^2$, $2/3 \leq 1 - \frac{h^2}{12} \lambda_j \leq 1$, $j \geq 1$. It is easy to show that the eigenvalues γ_j of operators \mathcal{L}_x and \mathcal{L}_y are given by $\gamma_j = 1 - \frac{h^2}{12} \lambda_j$, $j \geq 1$. Following the von Neumann method for linear stability analysis, we express the numerical solution to ADI scheme (9)–(10) by means of a Fourier sum $U_{jk}^n = \sum_{l=1}^{J-1} \sum_{m=1}^{K-1} c_{lm}^n Y_l(x_j) Y_m(y_k)$, where $Y_l(x) = \sqrt{2} \sin(l\pi x)$ are orthonormal eigenvectors. Substituting it into the ADI scheme, after simple computations we get

$$c_{lm}^{n+1} = \frac{\gamma_l \gamma_m - \frac{\tau^2}{4} \lambda_l (\lambda_m + q \gamma_m) - i \frac{\tau}{2} [\lambda_l \gamma_m + \gamma_l (\lambda_m + q \gamma_m)]}{\gamma_l \gamma_m - \frac{\tau^2}{4} \lambda_l (\lambda_m + q \gamma_m) + i \frac{\tau}{2} [\lambda_l \gamma_m + \gamma_l (\lambda_m + q \gamma_m)]} c_{lm}^n = \alpha_{lm}^n c_{lm}^n,$$

where α_{lm}^n is the amplification factor. Since $\lambda_l > 0$, $\gamma_l > 0$, it follows that $|\alpha_{lm}^n| = 1$, i.e. $|c_{lm}^{n+1}| = |c_{lm}^n|$, and therefore

$$(11) \quad \|U^{n+1}\|^2 = \sum_{l=1}^{J-1} \sum_{m=1}^{K-1} |c_{lm}^{n+1}|^2 = \sum_{l=1}^{J-1} \sum_{m=1}^{K-1} |c_{lm}^n|^2 = \|U^n\|^2.$$

Thus, we have proved that a discrete version of the conservation law (4) is satisfied for the discrete scheme (9)–(10). Moreover, the energy norm of the vector can be

computed as $\|U^n\|_E^2 = \sum_{l=1}^{J-1} \sum_{m=1}^{K-1} (\lambda_l + \lambda_m) |c_{lm}^n|^2$, and therefore, taking into account equalities (11) and $|c_{lm}^{n+1}| = |c_{lm}^n|$, we get

$$(12) \quad E_h^{n+1} = \|U^{n+1}\|_E^2 + q\|U^{n+1}\|^2 = \|U^n\|_E^2 + q\|U^n\|^2 = E_h^n.$$

Thus, a discrete version of the second conservation law (5) is also satisfied for the linear discrete scheme (9)–(10). We note that the accuracy of both discrete conservation laws, (11) and (12), was numerically tested in [15] even for linear test problems. It follows from the estimates given above that, in fact, both discrete conservation laws are exactly conserved for such examples.

In [15], the convergence of the solution of the discrete scheme (9)–(10) is proved only if the temporal and spatial discretization steps satisfy the relation $\tau < h^2/3$. We will prove that a conditional convergence estimate is obtained only due to the application of the energy estimates technique, and such restrictions on grid-steps are not necessary at least in the case of constant coefficients. Let $Z_{jk}^n = u_{jk}^n - U_{jk}^n$ be the global error. From (8) we get the following error problem

$$(13) \quad -i\left(\mathcal{L}_x - i\frac{\tau}{2}\partial_x^2\right)\left(\mathcal{L}_y - i\frac{\tau}{2}\left[\partial_y^2 - \mathcal{L}_y Q\right]\right)\partial_t Z_{jk}^n = \mathcal{L}_y \partial_x^2 Z_{jk}^n + \mathcal{L}_x \partial_y^2 Z_{jk}^n - \mathcal{L}_x \mathcal{L}_y q_{jk} Z_{jk}^n + R_{jk}^n,$$

$$(14) \quad Z_{jk}^0 = 0, \quad (x_j, y_k) \in \bar{\Omega}_h, \quad Z_{jk}^n = 0, \quad (x_j, y_k) \in \partial\Omega_h,$$

where R^n denotes the truncation error of order $\mathcal{O}(\tau^2 + h^4)$.

Next, we consider the linear case of equation (1).

Theorem 1. *Suppose that the exact solution $u(x, y, t)$ to the problem (1)–(3) is sufficiently smooth, $f = f(x, y, t)$ is a given function and $q(x, y, t) \equiv q$ is constant. Then, the solution of the linear ADI discrete scheme (9)–(10) converges to $u(x, y, t)$ and the following estimate is valid:*

$$(15) \quad \max_{1 \leq n \leq N} \|u^n - U^n\| \leq C(\tau^2 + h^4).$$

Proof. Let us represent the truncation error R^n and the global error Z^n as Fourier sums. Substituting them into equation (13), after simple computations we get the following discrete equation $z_{lm}^{n+1} = \alpha_{lm}^n z_{lm}^n + \tau \beta_{lm}^n r_{lm}^n$, where the amplification factor α_{lm}^n is defined above and

$$\beta_{lm}^n = i/(\gamma_l + i\frac{\tau}{2}\lambda_l)(\gamma_m + i\frac{\tau}{2}(\lambda_m + q)).$$

Since $\gamma_j \geq 2/3$, we conclude that $|\beta_{lm}^n| \leq 9/4$. As a result, we get the estimate $|z_{lm}^{n+1}| \leq |z_{lm}^n| + \frac{9}{4}\tau|r_{lm}^n|$. Using the triangle inequality for the L_2 norm of vectors and the relation between the norms of Fourier coefficients and error functions Z^n , we prove the stability estimate

$$\|Z^{n+1}\| \leq \|Z^n\| + \frac{9}{4}\tau\|R^n\|.$$

Summing up the obtained inequalities and using the initial condition (14), we prove the convergence of the solution of the linear ADI discrete scheme (9)–(10) to $u(x, y, t)$ and the estimate (15). \square

It is proved in [10] that the ADI scheme can not be generalized for 3D Schrödinger problems, since the stability of the scheme can not be guaranteed. In this case the Strang like LOD schemes can be used to derive the second order accurate approximations [10].

4. MG Solver

The focus of this section is to investigate the application of multigrid to the linear version of model problem (1).

The performance of geometric multigrid methods is strongly dependent on the choice of adequate components to the considered problem, and in this sense, we have to carefully choose the corresponding components for our concrete problem. First of all, a hierarchy of grids is necessary for the implementation of geometric multigrid. Here, it is obtained by applying standard coarsening to the considered target grid on which our problem is discretized. Once the hierarchy of grids is fixed, the two main components of multigrid algorithms are on the one hand the smoother, which has to efficiently eliminate high-frequency components of the error, and on the other hand the coarse-grid correction operator, which has to do the rest of the work. This latter is composed of the inter-grid transfer operators: restriction and prolongation, and the coarse-grid operator. All these components should be chosen so that they efficiently interplay with each other in order to obtain a good connection between the relaxation and the coarse-grid correction parts of the algorithm. In this work, the coarse-grid correction operator is chosen in a standard way within the framework of structured rectangular grids. Bilinear interpolation and full-weighting restriction are the considered inter-grid transfer operators, and the problem is directly discretized on coarser grids, which are obtained by doubling in each direction the grid-size of the finer grid.

Regarding the smoother, multicolor relaxation has been proven to be a very efficient choice as smoother for multigrid methods. The best known example of this kind of relaxation is the red-black Gauss-Seidel smoother. In this relaxation process, updated values are taken into account for the computation of the approximation on the current node, and the order in which grid-points are visited is in a chessboard or red-black manner. In this way, the unknowns with the same color have no connections among them for five-point-stencils, what makes this method to be well-suited for parallel computation. It is also well-known the advantages of this smoother over the classical lexicographic Gauss Seidel relaxation, since in addition to be more parallelizable, the provided convergence is more satisfactory. The chosen coarse grid correction components together with a red-black smoother compound an optimal geometric multigrid method for the Laplace problem on rectangular grids, what makes us to think that it will be a good choice for the considered problem.

4.1. Two- and three-grid local Fourier analysis. The local Fourier analysis (LFA), introduced by Brandt in 1977 [5], is a quantitative analysis for MG algorithms, in the sense that it provides accurate predictions of the asymptotic convergence rates of such methods. This analysis is based on the Fourier transform theory, and a good introduction can be found in the books by Trottenberg et al. [25], and Wienands and Joppich [26]. A k-level local Fourier analysis is a very useful tool to predict the convergence rate of a multigrid algorithm. The main idea of this analysis is formally to extend all multigrid components to an infinite grid, neglecting the boundary conditions, and to restrict the analysis to discrete linear operators with constant coefficients. Despite these restrictions, if boundary conditions are appropriately treated, in general this analysis matches the numerical results satisfactorily.

As previously commented, to perform LFA, the discrete problem $L_h u_h = f_h$ is extended to an infinite grid:

$$(16) \quad G_h = \{\mathbf{x} = (x_1, x_2) \mid x_i = k_i h_i, k_i \in \mathbb{Z}, i = 1, 2\},$$

where $\mathbf{h} = (h_1, h_2)$ is a grid spacing. Then, the basis for any of the approaches to LFA is that a grid-function $u_h(\mathbf{x}) \in (l_h^2(G_h))$ can be represented as a formal linear combination of the so-called Fourier modes $\varphi_h(\boldsymbol{\theta}, \mathbf{x}) = e^{i\theta_1 x_1} e^{i\theta_2 x_2}$, with $\mathbf{x} \in G_h$, and $\boldsymbol{\theta} = (\theta_1, \theta_2) \in \Theta_h = (-\pi/h_1, \pi/h_1] \times (-\pi/h_2, \pi/h_2]$, which give rise to the Fourier space:

$$\mathcal{F}(G_h) = \text{span}\{\varphi_h(\boldsymbol{\theta}, \cdot) \mid \boldsymbol{\theta} \in \Theta_h\}.$$

Therefore, since the discrete operator L_h satisfies the corresponding assumptions for LFA, Fourier modes $\varphi_h(\boldsymbol{\theta}, \mathbf{x})$ are formal eigenfunctions of L_h , and more precisely, it is fulfilled that $L_h \varphi_h(\boldsymbol{\theta}, \mathbf{x}) = \tilde{L}_h(\boldsymbol{\theta}) \varphi_h(\boldsymbol{\theta}, \mathbf{x})$, where $\tilde{L}_h(\boldsymbol{\theta})$ is the Fourier symbol of L_h . Using standard coarsening, high and low frequency components on G_h are distinguished, in the way that the subset of low frequencies is $\Theta_{2h} = (-\pi/2h_1, \pi/2h_1] \times (-\pi/2h_2, \pi/2h_2]$, and the subset of high frequencies is $\Theta_h \setminus \Theta_{2h}$.

Let u_h^m be an approximation of u_h . The error $e_h^m = u_h^m - u_h$ is transformed by a two-grid cycle as $e_h^{m+1} = M_h^{2h} e_h^m$, where $M_h^{2h} = S_h^{\nu_2} C_h^{2h} S_h^{\nu_1}$ is the two-grid operator, $C_h^{2h} = I_h - I_{2h}^h (L_{2h})^{-1} I_h^{2h} L_h$ the coarse grid correction operator and S_h is a smoothing operator on G_h with ν_1 and ν_2 indicating the number of pre- and post-smoothing steps, respectively. In the definition of C_h^{2h} , L_{2h} is the coarse grid operator and I_{2h}^h, I_h^{2h} are transfer operators from coarse to fine grids and vice versa. The two-grid analysis is the basis for the classical asymptotic multigrid convergence estimates, and the spectral radius $\rho(M_h^{2h})$ of the operator M_h^{2h} indicates the asymptotic convergence factor of the two-grid method.

In order to guarantee that nonsingular Fourier symbols $\tilde{L}_h(\boldsymbol{\theta})$ and $\tilde{L}_{2h}(2\boldsymbol{\theta})$ are taken, we restrict our considerations to $\tilde{\Theta}_{2h} = \Theta_{2h} \setminus \Psi$, with

$$\Psi = \{\boldsymbol{\theta}^{00} \in \Theta_{2h} \mid \det(\tilde{L}_{2h}(2\boldsymbol{\theta}^{00})) = 0, \text{ or } \det(\tilde{L}_h(\boldsymbol{\theta}^{ij})) = 0, i, j \in \{0, 1\}\},$$

where

$$\begin{aligned} \boldsymbol{\theta}^{10} &= \boldsymbol{\theta}^{00} - (\text{sign}(\theta_1^{00})\pi/h_1, 0), & \boldsymbol{\theta}^{01} &= \boldsymbol{\theta}^{00} - (0, \text{sign}(\theta_2^{00})\pi/h_2), \\ \boldsymbol{\theta}^{11} &= \boldsymbol{\theta}^{00} - (\text{sign}(\theta_1^{00})\pi/h_1, \text{sign}(\theta_2^{00})\pi/h_2), \end{aligned}$$

being θ_1^{00} and θ_2^{00} the coordinates of $\boldsymbol{\theta}^{00}$. As is well known, assuming standard coarsening, the coarse grid correction operator C_h^{2h} couples four Fourier components. Each low frequency $\boldsymbol{\theta}^{00} \in \tilde{\Theta}_{2h}$ is coupled with three high frequencies, $\boldsymbol{\theta}^{10}$, $\boldsymbol{\theta}^{01}$, and $\boldsymbol{\theta}^{11}$, as we can see in Figure 1. These frequencies compose the four-dimensional subspaces $\mathcal{F}^4(\boldsymbol{\theta}^{00})$ of $2h$ -harmonics, which remain invariant under C_h^{2h} . The same invariance property holds for many well-known smoothers, such the one considered in this work. Therefore, the two-grid operator $M_h^{2h} = S_h^{\nu_2} C_h^{2h} S_h^{\nu_1}$ also leaves the $2h$ -harmonic subspaces invariant, and as a consequence it can be represented by a block-diagonal matrix, consisting of (4×4) -blocks, denoted by

$$\widehat{M}_h^{2h}(\boldsymbol{\theta}^{00}) = (\widehat{S}_h(\boldsymbol{\theta}^{00}))^{\nu_2} \widehat{C}_h^{2h}(\boldsymbol{\theta}^{00}) (\widehat{S}_h(\boldsymbol{\theta}^{00}))^{\nu_1},$$

with $\boldsymbol{\theta}^{00} \in \tilde{\Theta}_{2h}$, and where the Fourier representation of the relaxation method is a (4×4) -matrix, $\widehat{S}_h(\boldsymbol{\theta}^{00})$, and the block-matrix representation of the coarse grid correction in the subspace $\mathcal{F}^4(\boldsymbol{\theta}^{00})$ is given by

$$\widehat{C}_h^{2h}(\boldsymbol{\theta}^{00}) = \widehat{I}_h - \widehat{I}_{2h}^h(\boldsymbol{\theta}^{00}) (\widehat{L}_{2h}(\boldsymbol{\theta}^{00}))^{-1} \widehat{I}_h^{2h}(\boldsymbol{\theta}^{00}) \widehat{L}_h(\boldsymbol{\theta}^{00}) \in \mathbb{C}^{4 \times 4},$$

being \widehat{I}_h , $\widehat{L}_{2h}(\boldsymbol{\theta}^{00})$, $\widehat{L}_h(\boldsymbol{\theta}^{00})$, $\widehat{I}_h^{2h}(\boldsymbol{\theta}^{00})$ and $\widehat{I}_{2h}^h(\boldsymbol{\theta}^{00})$ the Fourier representations in $\mathcal{F}^4(\boldsymbol{\theta}^{00})$ of the operators involved in the coarse grid correction. As a consequence, the spectral radius $\rho(M_h^{2h})$ can be calculated by means of the spectral radius of

(4×4) -matrices, so it is possible to determine the asymptotic two-grid convergence factor as:

$$(17) \quad \rho^{2g} = \rho(M_h^{2h}) = \max_{\theta^{00} \in \tilde{\Theta}_{2h}} \rho(\widehat{M}_h^{2h}(\theta^{00})).$$

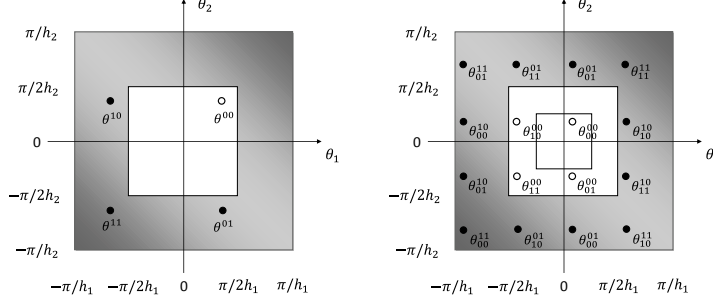


FIGURE 1. Frequencies coupled by a two-grid and a three-grid iteration, which generate the space of 2h- and 4h-harmonics.

Due to the recursivity of the definition of a k-grid method, the two-grid analysis introduced previously can be generalized to a k-grid analysis. Here, we are interested in a three-grid analysis, which is very useful to see the different performances of V- and W-cycles and the influence of different numbers of pre- and post-smoothing steps.

The error transformation by a three-grid cycle is given by $e_h^{m+1} = M_h^{4h} e_h^m$, with

$$M_h^{4h} = S_h^{\nu_2} C_h^{4h} S_h^{\nu_1} = S_h^{\nu_2} (I_h - I_{2h}^h (I_{2h} - (M_{2h}^{4h})^\gamma) (L_{2h})^{-1} I_h^{2h} L_h) S_h^{\nu_1},$$

where M_{2h}^{4h} is defined as

$$M_{2h}^{4h} = S_{2h}^{\nu_2} (I_{2h} - I_{4h}^{2h} (L_{4h})^{-1} I_{2h}^{4h} L_{2h}) S_{2h}^{\nu_1},$$

being γ the number of two-grid iterations (notice that $\gamma = 1$ corresponds to a V-cycle, whereas $\gamma = 2$ corresponds to a W-cycle).

In order to perform a three-grid analysis we have to take into account that not only in the transition from G_h to G_{2h} but also in the transition from G_{2h} to G_{4h} (where G_{2h} and G_{4h} are the coarse meshes, obtained by standard coarsening, and defined analogously to G_h in (16)), four Fourier frequencies are coupled, see Figure 1. Therefore, the three-grid operator couples 16 Fourier frequencies, which set up the subspaces of 4h-harmonics (composed of four subspaces of 2h-harmonics), $\mathcal{F}^{16}(\theta^{00})$, $\theta^{00} \in \tilde{\Theta}_{4h} = \Theta_{4h} \setminus \Psi_{4h}$, where $\Theta_{4h} = (-\pi/4h_1, \pi/4h_1] \times (-\pi/4h_2, \pi/4h_2]$, and $\Psi_{4h} = \{\theta^{00} \in \Theta_{4h} \mid \det(\tilde{\mathbf{L}}_{4h}(4\theta^{00})) = 0, \text{ or } \det(\tilde{\mathbf{L}}_{2h}(2\theta_{ij}^{00})) = 0, \text{ or } \det(\tilde{\mathbf{L}}_h(\theta_{nm}^{ij})) = 0, i, j, n, m \in \{0, 1\}\}$, where

$$\begin{aligned} \theta_{ij}^{00} &= \theta^{00} - (i\pi \operatorname{sign}(\theta_1^{00})/2h_1, j\pi \operatorname{sign}(\theta_2^{00})/2h_2) \\ \theta_{nm}^{ij} &= \theta_{nm}^{00} - (i\pi \operatorname{sign}((\theta_{nm}^{00})_1)/h_1, j\pi \operatorname{sign}((\theta_{nm}^{00})_2)/h_2). \end{aligned}$$

Hence, this operator can be represented in Fourier space by a block matrix consisting of (16×16) -blocks, and analogously to the definition of the asymptotic convergence factor for the two-grid analysis, we can define it for the three-grid analysis as

$$(18) \quad \rho^{3g} = \rho(M_h^{4h}) = \max_{\theta^{00} \in \tilde{\Theta}_{4h}} \rho(\widehat{M}_h^{4h}(\theta^{00})).$$

Next, some results of the three-level analysis for the linear Schrödinger equation are shown.

4.2. Local Fourier analysis results. In this section, we present results from a three-grid LFA for schemes (6) and (7), in the case of $q(x, y, t) = 0$, and $f(u) = 0$, by using a V-cycle with one pre- and one post-smoothing steps and the previously proposed components of the multigrid method. In the case of the high-order scheme in space, low-order schemes (6) are chosen on coarse grids.

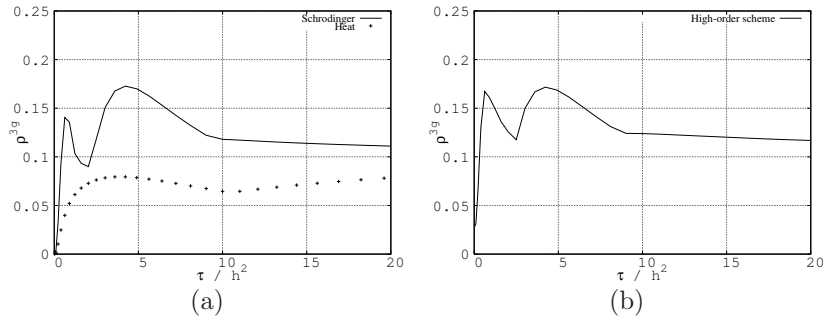


FIGURE 2. Three-level LFA for Schrödinger and parabolic heat equation for (a) scheme (6) and for (b) scheme (7).

For both schemes, we have performed a systematic three-grid LFA analysis for the proposed multigrid algorithm. For this problem, the asymptotic convergence factors are independent on τ/h^2 , as expected. In Figure 2 (a) the convergence factors predicted by the three-grid analysis, ρ^{3g} , for scheme (6) are shown for a wide range of values of τ/h^2 . As it is seen, these factors are almost independent when the parameter τ/h^2 is bigger than about 10, expecting the optimal complexity estimate of multigrid. In the opposite case, that is, when the parameter is lower than this value, we observe that the convergence rate could vary from 0.09 to 0.17. From the practical point of view, this dependence could imply an unexpected behavior of the classical multigrid algorithm. In the same picture, we have included the same analysis for the well-known parabolic heat equation, discretized by the Crank-Nicolson scheme, in order to see the difference in the behavior of multigrid. In Figure 2 (b), we show the corresponding analysis performed for the high-order scheme (7). We observe a similar behavior as for the low-order scheme, that is, dependent convergence factors for small values of τ/h^2 , and almost independent convergence factors when this parameter is big enough.

In order to test if the proposed MG version of the solver remains robust and efficient for 3D problems, we also have performed a two-grid LFA analysis for the 3D version of the Crank-Nicolson scheme. In Figure 3 the convergence factors predicted by the two-grid analysis for the 2D scheme (6) and for the 3D version of this scheme are shown for a wide range of values of τ/h^2 . In the case of the 3D scheme, we observe a monotonic behavior of the convergence factor for small values of τ/h^2 , and almost independent convergence factors when this parameter is big enough. Thus the theory predicts that the MG solver is a robust and efficient solver for 3D Schrödinger equations.

5. Numerical Experiments

In this section, the efficiency of the three considered solvers is tested. Our main goal is not to investigate the accuracy of the proposed finite difference schemes

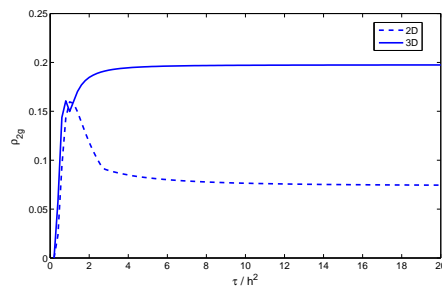


FIGURE 3. Two-level LFA for the 2D and 3D Crank-Nicolson scheme (6) for the Schrödinger equation.

(such analysis is done in many papers), but to test the efficiency of the MG solver and to compare it with the direct ADI and FFT solvers. For this purpose, we use examples proposed in [15].

Computations were performed on Vilkas cluster of computers at Vilnius Gediminas Technical University, consisting of nodes with Intel®Core™ processor i7-860 @ 2.80 GHz and 4 GB DDR3-1600 RAM. FFT algorithm was implemented by using the well-known library FFTW.

Example 1. We consider the linear Schrödinger equation (1) with potential $q(x, y, t) \equiv 0$ and $f(u) \equiv 0$. The exact solution is given by (note, that a small error is done in [15])

$$u(x, y, t) = \frac{i}{i - 4t} \exp \left[-i((x-1)^2 + (y-1)^2 + ik(x-1) + ik^2t)/(i-4t) \right],$$

where $(1, 1)$ is the initial center of a transient Gaussian wave, and $k = 2.5$ is the wave number. We simulate the movement of a wave in the domain $[-10, 10] \times [-10, 10]$, till time $T = 1$. The initial conditions are computed from the exact solution and zero boundary conditions are specified.

The complexity of the considered direct algorithms, i.e. FFT and ADI methods, do not depend on the time step τ . Thus, for these solvers, we have used a relation $\tau = Ch$ for temporal and spatial mesh-steps. Table 1 reports CPU times in seconds for the solution of the discrete problem with different mesh-sizes. The FFT algorithm is applied for the symmetrical finite difference scheme (6), but very similar CPU times are obtained for the high-order approximation compact Crank-Nicolson scheme (7). The results of the computational experiments are in good agreement with the

TABLE 1. CPU times for the solution of Example 1 till $T = 1$, with ADI scheme (8) and FFT implementation of the symmetrical finite difference scheme (6). A sequence of step-sizes is used with $\tau = 1/N$ and $h = 20/J$.

Algorithm	$J = 128$ $N = 50$	$J = 256$ $N = 100$	$J = 512$ $N = 200$	$J = 1024$ $N = 400$
ADI	0.122	1.03	8.9	72.3
FFT	0.37	3.19	27.2	231.8

theoretical complexity estimates $\mathcal{O}(N^3)$ for ADI algorithm and $\mathcal{O}(N^3 \log N)$ for FFT algorithm.

Next we have solved the same problem by using the finite difference scheme (6) and the proposed MG solver. Table 2 presents CPU times and asymptotic convergence rates predicted by LFA for different mesh-sizes. The stopping criterion is chosen as the maximum residual to be less than $\varepsilon = 10^{-4}$. The results of the

TABLE 2. CPU times for the solution of Example 1 till $T = 1$ and asymptotic convergence rates predicted by LFA are given for the MG implementation of the symmetrical finite difference scheme (6). A sequence of step-sizes is used with $\tau = 1/N$ and $h = 20/J$, and the stopping criterion is defined by $\varepsilon = 10^{-4}$.

	$N = 50$	$N = 100$	$N = 200$	$N = 400$	$N = 800$
$J=128$	0.62 (0.14)	0.98 (0.1)	1.33 (0.02)	2.56 (4E-3)	3.12 (5E-4)
$J=256$	2.47 (0.16)	3.81 (0.09)	8.82 (0.14)	15.1 (0.09)	21.4 (0.02)
$J=512$	10.2 (0.11)	16.2 (0.15)	36.8 (0.16)	49.6 (0.09)	126 (0.14)

computational experiments show that the efficiency of MG solver is quite similar to that of FFT solver. For the chosen stopping criterion ($\varepsilon = 10^{-4}$), the convergence rate of MG is even better than the theoretical predictions obtained by LFA. But, asymptotically, for small values of ε , the experimental results are in very good agreement with the theoretical predictions. For example, we present some experimental values of asymptotic convergence rates for $\varepsilon = 10^{-8}$, $J = 256$ and different time steps:

$$\rho(50) = 0.13, \quad \rho(100) = 0.09, \quad \rho(200) = 0.135, \quad \rho(400) = 0.09.$$

These results show that the three-grid local Fourier analysis gives very accurate predictions of the convergence rates of the MG algorithm. The dependence of the convergence rate on time step τ is non-monotonous in the region of interest.

In Table 3, we present results of computational experiments when the same problem is solved by using MG solver for the high-order finite difference scheme (7). Again, the stopping criterion is chosen as the maximum residual to be less than $\varepsilon = 10^{-4}$. It follows from the presented results that the MG solver is quite robust with

TABLE 3. CPU times for the solution of Example 1 till $T = 1$ and asymptotic convergence rates predicted by LFA are given for the MG implementation of the high-order finite difference scheme (7). A sequence of step-sizes is used with $\tau = 1/N$ and $h = 20/J$, and the stopping criterion is defined by $\varepsilon = 10^{-4}$.

	$N = 50$	$N = 100$	$N = 200$	$N = 400$	$N = 800$
$J=128$	0.94 (0.16)	1.54 (0.13)	2.28 (0.06)	3.88 (0.03)	7.75 (0.03)
$J=256$	3.64 (0.16)	5.58 (0.13)	13.9 (0.16)	22.3 (0.13)	34.2 (0.06)
$J=512$	14.7 (0.12)	23.4 (0.15)	52.5 (0.16)	71.9 (0.13)	185 (0.16)

respect to various difference approximations of the 2D Schrödinger equation. Again, the experimental results are in very good agreement with theoretical predictions of the convergence rates given by the three-grid local Fourier analysis.

Example 2. We consider the linear Schrödinger equation

$$-i\frac{\partial u}{\partial t} = \frac{\partial^2 u}{\partial x^2} + \frac{\partial^2 u}{\partial y^2} + (3 - 2 \tanh^2(x) - 2 \tanh^2(y))u$$

in the domain $[0, 1] \times [0, 1]$. The problem is solved till $T = 1$, and the exact solution is given as $u(x, y, t) = \frac{i \exp(it)}{\cosh(x) \cos(y)}$. The initial and boundary conditions are obtained from the exact solution.

The main aim of this example is to study the robustness of the MG solver with respect to non-constant potential coefficients. Some CPU times are presented in Table 4, in which the stopping criterion is chosen as the maximum residual to be less than $\varepsilon = 10^{-4}$.

TABLE 4. CPU times for the solution of Example 2 till $T = 1$ with the MG implementation of the finite difference scheme (6). A sequence of step-sizes is used with $\tau = 1/N$ and $h = 1/J$, and the stopping criterion is defined by $\varepsilon = 10^{-4}$.

	$N = 50$	$N = 100$	$N = 200$	$N = 400$	$N = 800$
$J = 128$	0.92	1.63	2.98	4.69	9.52
$J = 256$	3.81	7.67	12.4	24.9	38.7
$J = 512$	18.8	31.8	63.3	105	207

It follows from the presented results that the MG solver is robust with respect to the inclusion of the potential function, and therefore it can be recommended for the solution of more general nonlinear 2D Schrödinger equations.

Example 3. In this example we consider the non-linear Schrödinger equation

$$(19) \quad -i\frac{\partial u}{\partial t} = \frac{\partial^2 u}{\partial x^2} + \frac{\partial^2 u}{\partial y^2} + g(u)u$$

in the domain $[0, 2\pi] \times [0, 2\pi]$. This problem is approximated by the Crank-Nicolson finite difference scheme (6) and the following iterative algorithms are used: the explicit iterative method

$$(20) \quad -i\partial_t U_{jk}^{n,s} = \partial_x^2 U_{jk}^{n+\frac{1}{2},s} + \partial_y^2 U_{jk}^{n+\frac{1}{2},s} + g(U_{jk}^{n+\frac{1}{2},s-1})U_{jk}^{n+\frac{1}{2},s-1}$$

and the semi-implicit iterative method

$$(21) \quad -i\partial_t U_{jk}^{n,s} = \partial_x^2 U_{jk}^{n+\frac{1}{2},s} + \partial_y^2 U_{jk}^{n+\frac{1}{2},s} + g(U_{jk}^{n+\frac{1}{2},s-1})U_{jk}^{n+\frac{1}{2},s}.$$

Note that the FFT algorithm can be used only for the explicit iterative algorithm (20), whereas the MG solver can be used for both approaches.

We assume that g is a real valued function and it satisfies estimates

$$|g(v)| \leq M_0, \quad |g(v) - g(w)| \leq M_1|u - v|$$

for any functions v, w in some neighbourhood of the exact solution $B_R(u)$. In order to simplify the details of the convergence analysis, we restrict to the iterative algorithms for the split type scheme, when the nonlinear interaction and the linear diffraction processes are treated separately. Thus instead of (20) for each $(x_j, y_k) \in \Omega_h$ we consider the discrete problem

$$(22) \quad \partial_t U_{jk}^{n,s} = ig(U_{jk}^{n+\frac{1}{2},s-1})U_{jk}^{n+\frac{1}{2},s-1}$$

Let us denote the error $Z_{jk}^s = U_{jk}^{n+1} - U_{jk}^{n+1,s}$. We get the following error equation

$$\begin{aligned} Z_{jk}^s &= i\tau \left(g(U_{jk}^{n+\frac{1}{2}}) U_{jk}^{n+\frac{1}{2}} - g(U_{jk}^{n+\frac{1}{2},s-1}) U_{jk}^{n+\frac{1}{2}} \right. \\ &\quad \left. + g(U_{jk}^{n+\frac{1}{2},s-1}) U_{jk}^{n+\frac{1}{2}} - g(U_{jk}^{n+\frac{1}{2},s-1}) U_{jk}^{n+\frac{1}{2},s-1} \right) \end{aligned}$$

from which by using the Taylor series we prove the estimate

$$|Z_{jk}^s| \leq \frac{\tau}{2} (M_0 + M_1 |U^{n+\frac{1}{2}}|) |Z_{jk}^{s-1}|.$$

Thus the convergence factor of the explicit iterative algorithm (20) can be estimated as $\rho_E = \frac{\tau}{2} (M_0 + M_1 \|U^{n+\frac{1}{2}}\|_\infty)$.

The convergence factor of the semi-implicit iterative algorithm (21) is derived in a similar way by considering the discrete problem

$$\partial_t U_{jk}^{n,s} = ig(U_{jk}^{n+\frac{1}{2},s-1}) U_{jk}^{n+\frac{1}{2},s}.$$

Then we get the convergence factor $\rho_{SI} = \frac{\tau}{2} M_1 \|U^{n+\frac{1}{2}}\|_\infty$.

If $M_1 \|U^{n+\frac{1}{2}}\|_\infty \ll M_0$, the semi-implicit iterative algorithm (21) is much more effective than the explicit algorithm. For example, such a situation occurs when $g = g(x)$ is a non-constant given function, then $M_1 = 0$ and the semi-implicit algorithm requires only one iteration.

Here we mention one interesting non-iterative scheme, which is proposed by C. Besse [3]. Instead of iterations in Crank-Nicolson scheme (21) the nonlinearity is resolved by using the staggered time grid:

$$(23) \quad \begin{cases} \frac{\Phi_{jk}^{n+\frac{1}{2}} + \Phi_{jk}^{n-\frac{1}{2}}}{2} = g(U_{jk}^n), \\ -i\partial_t U_{jk}^n = \left(\partial_x^2 + \partial_y^2 \right) \frac{U_{jk}^{n+1} + U_{jk}^n}{2} + \Phi_{jk}^{n+\frac{1}{2}} \frac{U_{jk}^{n+1} + U_{jk}^n}{2}, \end{cases}$$

where the real valued function $\Phi^{n+\frac{1}{2}}$ is defined on a staggered time grid $\{t^{n-\frac{1}{2}}, n = 0, \dots, N\}$ with the initial data $\Phi^{-\frac{1}{2}}(x) = g(u^0(x))$. Thus with respect to the MG solver, the nonlinearity of the Schrödinger differential equation can be interpreted as a given potential function (see Example 2).

As an example, we consider the non-linear Schrödinger equation with a nonlinear function $g(u) = |u|^2$:

$$(24) \quad -i\frac{\partial u}{\partial t} = \frac{\partial^2 u}{\partial x^2} + \frac{\partial^2 u}{\partial y^2} + |u|^2 u$$

in domain $[0, 2\pi] \times [0, 2\pi]$. The exact solution describes a progressive plane wave $u(x, y, t) = \exp(-i(x+y+t))$. A simple analysis shows that for this problem the explicit and semi-implicit iterative algorithms converge with a similar rate. Thus, this example gives us one more possibility to investigate the robustness of the MG solver with respect to the perturbations of the matrix by non-constant potential coefficients.

In Table 5 we present the results of computational experiments when problem (24) is solved by using the MG solver for the explicit iterative algorithm (20) and the semi-implicit iterative algorithm (21). The stopping criterion for the MG iterations is chosen as the maximum residual to be less than $\varepsilon = 10^{-4}$ and for the nonlinear iterations $\varepsilon_1 = 10^{-3}$.

It follows from the presented results that the MG solver is robust with respect to the semi-implicit iterative algorithm.

TABLE 5. The global CPU times and the average numbers of non-linear iterations per time step for the solution of Example 3 till $T = 1$ with the MG implementation of the explicit iterative algorithm (20) (first two rows) and the semi-implicit iterative algorithm (21) (last two rows). A sequence of step sizes is used with $\tau = 1/N$ and $h = 2\pi/J$, and the stopping criterion is defined by $\varepsilon = 10^{-4}$.

	$N = 50$	$N = 100$	$N = 200$	$N = 400$	$N = 800$
$J = 128$	1.71 (8)	3.38 (8)	5.83 (7)	12.1 (7)	24.6 (7)
$J = 256$	7.37 (9)	13.6 (8)	23.3 (7)	46.5 (7)	82.8 (6)
$J = 128$	3.36 (10)	7.38 (11)	11.6 (9)	24.7 (9)	55.0 (10)
$J = 256$	15.8 (11)	36.8 (12)	53.6 (9)	134.8 (11)	229.7 (9)

The parallelization of the ADI type methods can be done by using the domain decomposition method. The main challenge is to solve in parallel systems of linear equations with tridiagonal matrices. On the basis of theoretical and experimental analysis done in [7] we recommend to use the Wang factorization algorithm. The results of computational experiments for 2D diffusion problems have confirmed the predictions of the theoretical scalability analysis. The parallel versions of the FFT algorithm are included into the FFTW library and are based on the optimized parallel matrix transpose operator. The parallelization of the MG algorithm can be done in standard way by using the domain decomposition method. The main part of computations is done during the implementation of the smoother operator and this part can be parallelized very efficiently, see [8].

6. Conclusions

A comparison of different solvers and different approaches for the numerical solution of Schrödinger problems is dealt with in this work. Two finite difference schemes based on the Crank-Nicolson approach have been considered to approximate the problem. One of them, consists of a high-order compact scheme, for which an ADI type decomposition is formulated. The stability and convergence of this approach are investigated and some estimates are provided. The considered solvers for comparison are based on the multigrid geometric methods, FFT method and the ADI solver. These algorithms have been tested for a linear Schrödinger problem, proving that the computational experiments are in good agreement with the theoretical predictions. In order to test the robustness of the MG solver two additional Schrödinger problems with a non-constant potential and nonlinear right-hand side are solved by the MG solver, since the efficiency of this solver depends on such data. The multigrid method results are quite robust with respect to various difference approximations of the two-dimensional linear Schrödinger equation, and it can be recommended as a general solver for nonlinear Schrödinger problems.

Acknowledgments

The authors would like to thank the referees for their constructive criticism which helped to improve the clarity and quality of this note.

The work of R. Čiegis was supported by Eureka project E!6799 POWEROPT "Mathematical modelling and optimization of electrical power cables for an improvement of their design rules".

References

- [1] G.D. Akrivis, V.D. Dougalis, and V.A. Karakashian, On fully discrete Galerkin methods of second-order temporal accuracy for the nonlinear Schrödinger equation, *Numer. Math.*, 59:31–53, 1991.
- [2] X. Antoine, A. Arnold, Ch. Besse, M. Ehrhardt, and A. Schädle, A review of transparent and artificial boundary conditions techniques for linear and nonlinear Schrödinger equations, *Commun. in Comput. Physics*, 4(4):729–796, 2008.
- [3] C. Besse, A relaxation scheme for the nonlinear Schrödinger equation, *SIAM J. Numer. Anal.*, 42(3):934–952, 2004.
- [4] C. Besse, B. Bidegaray, and S. Descombes, Order estimates in time splitting methods for the nonlinear Schrödinger equation, *SIAM J. Numer. Anal.*, 40:26–40, 2002.
- [5] A. Brandt, Multi-level adaptive solutions to boundary-value problems, *Math. Comput.*, 31:333–390, 1977.
- [6] R. Čiegis, A symmetrical decomposition scheme for a Schrödinger problem, *Diff. Eq.*, 39(7):1044–1049, 2003.
- [7] R. Čiegis, A. Bugajev, Parallel numerical algorithms for simulation of multidimensional imposed nonlinear diffusion-advection-reaction models. Editors: Manninen, Pekka; Oster, Per. In: *Lecture Notes Computer Science (LNCS), PARA2012. Subseries: Theoretical Computer Science and General Issues Proceedings of 11th International Conference, PARA 2012, Helsinki, Finland, June 13–15, 2012, Volume 7782, 387–397, 2013.*
- [8] R. Čiegis, F. Gaspar, C. Rodrigo, Parallel multiblock multigrid algorithms for poroelastic models, In: (R. Čiegis, D. Henty, Bo Kagstrom, J. Žilinskas, Eds.), *Parallel Scientific Computing and Optimization. Advances and Applications. Springer Optimization and Its Applications. Volume 27, 169–180, 2009.*
- [9] R. Čiegis, I. Laukaitytė, and M. Radziunas, Numerical algorithms for Schrödinger equations with absorbing boundary conditions, *Nonlinear Functional Analysis and Optimization*, 30(9–10):903–923, 2009.
- [10] R. Čiegis, A. Mirinavičius, M. Radziunas, Comparison of split step solvers for multidimensional Schrödinger problems, *Comp. Meth. Appl. Math.*, 13(2):237–250, 2013.
- [11] R. Čiegis and M. Radziunas, Effective numerical integration of traveling wave model for edge-emitting broad-area semiconductor lasers and amplifiers, *Math. Model. Anal.*, 15(4):409–430, 2010.
- [12] J. Cooley and J. Tukey, An algorithm for the machine computation of the complex fourier series, *Mathematics of Computation*, 19:297–301, 1965.
- [13] P. Duhamel and M. Vetterly, Fast fourier transforms: A tutorial review and a state of the art, *Signal Processing*, 19:259–299, 1990.
- [14] H.R. Elman, O.G. Ernst, and D.P. O’Leary, A multigrid method enhanced by Krylov subspace iteration for discrete Helmholtz equation, *SIAM J. Sci. Comput.*, 23(4):1291–1315, 2001.
- [15] Z. Gao and S. Xie, Fourth-order alternating direction implicit compact finite difference schemes for two-dimensional Schrödinger equations, *Appl. Numer. Math.*, 61:593–614, 2011.
- [16] W. Hundsdorfer and J.G. Verwer, *Numerical Solution of Time-Dependent Advection-Diffusion-Reaction Equations*, volume 33 of Springer Series in Computational Mathematics, Springer, Berlin, Heidelberg, New York, Tokyo, 2003.
- [17] J.C. Kalita, P. Chhabra, and S. Kumar, A semi-discrete higher order compact scheme for the unsteady two-dimensional Schrödinger equation, *J. Comput. Appl. Math.*, 197:141–149, 2006.
- [18] H. Knibbe, C.W. Oosterlee, and C. Vuik, GPU implementation of Helmholtz Krylov solver preconditioned by shifted Laplace multigrid method, *J. Comput. Appl. Maths.*, 236:281–293, 2011.
- [19] C. Lubich, On splitting methods for Schrödinger–Poisson and cubic nonlinear Schrödinger equations, *Math. Comput.*, 77:2141–2153, 2008.
- [20] A.A. Samarskii, *The Theory of Difference Schemes* Marcel Dekker, Inc., New York–Basel, 2001.
- [21] J. M. Sanz-Serna and J. G. Verwer, Conservative and non-conservative schemes for the solution of the nonlinear Schrödinger equation, *IMA J. Numer. Anal.*, 6(1):25–42, 1986.
- [22] G. Strang, On the construction and comparison of difference schemes, *SIAM J. Numer. Anal.*, 5:506–517, 1968.
- [23] T.R. Taha and M.J. Ablowitz, Analytical and numerical aspects of certain nonlinear evolution equations. II. Numerical Schrödinger equation, *J. Comp. Phys.*, 55:203–230, 1994.

- [24] M. Thalhammer, M. Caliari, and C. Neuhauser, High-order time-splitting Hermite and Fourier spectral methods, *J. Comput. Phys.*, 228:822–832, 2009.
- [25] U. Trottenberg, C.W. Oosterlee, and A. Schüller, *Multigrid*, Academic Press, New York, 2001.
- [26] R. Wienands and W. Joppich, *Practical Fourier analysis for multigrid methods*, Chapman and Hall/CRC Press, 2005.
- [27] F. Zhang, V.M. Pérez-García, and L. Vázquez, Numerical simulation of nonlinear Schrödinger systems: a new conservative scheme, *Appl. Math. Comput.*, 71:165–177, 1995.

IUMA, Departamento de Matematica Aplicada, Universidad de Zaragoza,, 50009 Zaragoza, Spain

E-mail: `fjgaspar@unizar.es` and `carmenr@unizar.es`

Vilnius Gediminas Technical University, Saulėtekio al. 11, LT-10223 Vilnius, Lithuania

E-mail: `rc@vgtu.lt` and `amirnavicius@gmail.com`